# Structure and Adsorption of A Hard-Core Multi-Yukawa Fluid Confined in A Slitlike Pore: Grand Canonical Monte Carlo Simulation and Density Functional Study

**Yang-Xin Yu* and Feng-Qi You**

*Department of Chemical Engineering, Tsinghua University, Beijing 100084, P. R. China and State Key Laboratory of Chemical Engineering, Tsinghua University, Beijing 100084, P. R. China*

**Yiping Tang**

*Honeywell Process Solutions, 300-250 York Street, London, Ontario, Canada N6A 6K2*

**Guang-Hua Gao and Yi-Gui Li**

*Department of Chemical Engineering, Tsinghua University, Beijing 100084, P. R. China*

*Received: September 19, 2005; In Final Form: November 7, 2005*

Because of the increasing interest in studying the phenomenon exhibited by charge-stabilized colloidal suspensions in confining geometry, we present a density functional theory (DFT) for a hard-core multi-Yukawa fluid. The excess Helmholtz free-energy functional is constructed by using the modified fundamental measure theory and Rosenfeld's perturbative method, in which the bulk direct correlation function is obtained from the first-order mean spherical approximation. To validate the established theory, grand canonical ensemble Monte Carlo (GCMC) simulations are carried out to determine the density profiles and surface excesses of multi-Yukawa fluid in a slitlike pore. Comparisons of the theoretical results with the GCMC data suggest that the present DFT gives very accurate density profiles and surface excesses of multi-Yukawa fluid in the slitlike pore as well as the radial distribution functions of the bulk fluid. Both the DFT and the GCMC simulations predict the depletion of the multi-Yukawa fluid near a nonattractive wall, while the mean-field theory fails to describe this depletion in some cases. Because the simple form of the direct correlation function is used, the present DFT is computationally as efficient as the mean-field theory, but reproduces the simulation data much better than the mean-field theory.

## I. Introduction

Understanding the structure and adsorption of fluids near solid surfaces is relevant to many traditional applications such as gas storage, oil recovery, heterogeneous catalyst reactions, removal of various pollutants, and fabrication of colloid-based nanostructured materials.[1−3] The interplay between intermolecular forces and external potential from solid surfaces makes the behavior of these confined fluids of interest but difficult to predict. Apart from the external potential, the intermolecular interaction is the only factor that affects the structure of fluids and the phenomena at the surface, such as adsorption, wetting, capillary condensation, etc.[4]

The various interactions between atoms and molecules can be calculated by using quantum mechanics, although such calculations are far from trivial, requiring electron correlation and large basis sets. In practice, we require some means to accurately model the interatomic potential curve using a simple empirical expression that can be rapidly calculated. Subsequently, the intermolecular interaction for an atomic fluid is usually modeled by using a Lennard−Jones potential term for van der Waals interactions and a Coulomb potential term for electrostatic interactions.[5] The Lennard−Jones potential, as pointed out by Tang et al.,[6] can be well approximated by a hard-core repulsion with two-Yukawa tails. A charged colloidal particle system interacting with a short-range attraction and a long-range electrostatic repulsion has been successfully described in the well-known Derjaguin−Laudan−Verwey−Overbeek (DLVO) theory,[7] which is also expressed as a Yukawa potential. For example, the hard-core two-Yukawa potential has been used to predict the thermodynamic and diffusion properties of bovine serum albumin (BSA) in aqueous electrolyte solution[8,9] and to explain the small-angle neutron scattering spectra of cytochrome C protein solutions at moderate concentrations.[10] Besides, the phase behavior of $C_{60}$ molecular systems and stability of colloidal dispersions has been accurately reproduced by using the hard-core two-Yukawa model.[11,12] In principle, the hard-core repulsion with three or more Yukawa tails can be used to approximate the intermolecular potential by including van der Waals interactions[13] and electrostatic interactions.[14] Therefore, we believe that the fluids with multi-Yukawa potentials should be able to simulate real systems without losing generality.

Because of the analytical availability and simplicity in solving the Ornstein−Zernike integral equation with the mean spherical approximation (MSA) closure, the phase equilibria, thermodynamic, and structural properties of the attractive hard-core one-Yukawa fluids and their mixtures have been investigated extensively.[15−26] The repulsive hard-core one-Yukawa fluid[27] and the multi-Yukawa fluid[28−30] also have received attention in recent years for their important applications to protein systems and colloidal suspensions.[10,31] In addition to the MSA-based

* To whom correspondence should be addressed. E-mail: yangxyu@mail.tsinghua.edu.cn.

10.1021/jp055299s CCC: $33.50 
Published on Web 12/09/2005

variations, there are achievements for the thermodynamics based on the Barker−Henderson perturbation theory using hard spheres as the reference.[27,32] The disadvantage of the perturbation theory is its absence of structural information. For the inhomogeneous case, the situation is different. The previous investigations[7,33−37] were concerned in the attractive and repulsive hard-core one-Yukawa fluid. There is no report on the inhomogeneous hard-core multi-Yukawa fluid up to now. Analysis of the previous theoretical investigations results in two groups of methods: one is integral equation theory and another is density functional theory (DFT). It proves that the DFT is more powerful than the integral equation theory in the prediction of the structural properties of inhomogeneous Yukawa fluids.[35]

The key task in a DFT is to construct the expression of the Helmholtz free-energy functional. Generally, the modified fundamental measure theory (MFMT)[38,39] yields very accurate density profiles for the hard-sphere fluids and their mixtures near walls and in slitlike pores. The remaining problem is how to handle the dispersion force contribution to the Helmholtz free-energy functional. The most simple and popular method for this problem is the so-called mean-field (MF) theory,[4] which is computationally efficient but describes some inhomogeneous phenomena only qualitatively. Efforts to improve the MF theory have been made by adopting the so-called effective reference field or the effective external potential.[40−42] The approach has successfully addressed interfacial and hydrophobic phenomena in inhomogeneous fluids, which is hardly expected from a traditional MF theory. An alternative way to correct the MF theory is to use the bulk direct correlation function (DCF) obtained from the integral equation theory. The analytical form of DCF was first generalized to the case of a multi-Yukawa potential by Hoye and Blum.[29] The correct coefficients of the analytical form have to be obtained by solving a group of nonlinear equations, and the complexity is increased with the number of terms in the multi-Yukawa potential. In contrast, the first-order mean spherical approximation (FMSA) solution obtained by Tang et al.[43] is straightforwardly a linear combination of individual one-Yukawa solutions, and has been applied to homogeneous three- and four-Yukawa fluids.[44] Because the analytical form of DCF from the FMSA is much simpler than that from the full MSA, the FMSA is adopted here to retrieve the fluid structure.

In this work, we reformulate the Helmholtz free-energy functional for the inhomogeneous hard-core multi-Yukawa fluid through Rosenfeld's perturbative method. The excess Helmholtz free-energy functional due to hard-sphere repulsion is evaluated from the MFMT, and dispersion contribution is approximated by using a quadratic expansion of the residual Helmholtz free-energy functional with respect to that for a uniform fluid of the same chemical potentials. Then the theory is applied to investigating the structure and adsorption of the hard-core multi-Yukawa fluid in a slitlike pore as well as the radial distribution function (RDF) of bulk multi-Yukawa fluid. To test the performance of the established DFT, grand canonical ensemble Monte Carlo (GCMC) simulations have been carried out to obtain the density profiles and adsorption isotherms of the hard-core multi-Yukawa fluid in the slitlike pore at different temperatures and densities. In the following section, we present the DFT for multi-Yukawa fluid. We briefly describe the simulation method in Section III. We present and discuss the numerical results for the density profiles, surface excesses, and RDF in Section IV, and we end with some conclusions in Section V.

## II. Density Functional Theory

The hard-core Yukawa (HCY) potential with multiple tails is given by

$$u(r) = \begin{cases} \infty & r \le \sigma \\ -\sum_{i=1}^{M} \dfrac{\epsilon_i \exp[-\lambda_i(r-\sigma)/\sigma]}{r/\sigma} & r > \sigma \end{cases} \tag{1}$$

where $\sigma$ is the diameter of particles, $r$ is the center-to-center distance between two interacting particles, $M$ is the number of tails, $\epsilon_i$ and $\lambda_i$ represent, respectively, the potential energy at contact and the screening length of Yukawa tail $i$.

In a density functional theory for an inhomogeneous hard-core multi-Yukawa fluid, the grand potential functional $\Omega[\rho(\mathbf{r})]$ is related to the Helmholtz energy functional $F[\rho(\mathbf{r})]$ via a Legendre transform,

$$\Omega[\rho(\mathbf{r})] = F[\rho(\mathbf{r})] + \int [V^{\text{ext}}(\mathbf{r}) - \mu]\rho(\mathbf{r})\, d\mathbf{r} \tag{2}$$

where $\rho(\mathbf{r})$ is the equilibrium density distribution, $V^{\text{ext}}(\mathbf{r})$ is the external field, and $\mu$ is the chemical potential of the fluid.

The Helmholtz energy functional $F[\rho(\mathbf{r})]$ can be formally expressed as an ideal-gas contribution $F^{\text{id}}[\rho(\mathbf{r})]$ plus an excess term $F^{\text{ex}}[\rho(\mathbf{r})]$ that accounts for the hard-sphere repulsion and van der Waals attraction,

$$F[\rho(\mathbf{r})] = F^{\text{id}}[\rho(\mathbf{r})] + F^{\text{ex}}[\rho(\mathbf{r})] \tag{3}$$

The ideal-gas contribution to the Helmholtz energy functional is exactly known as

$$F^{\text{id}}[\rho(\mathbf{r})] = kT \int d\mathbf{r}\rho(\mathbf{r})[\ln(\rho(\mathbf{r})\Lambda^3) - 1] \tag{4}$$

where $k$ is the Boltzmann constant, $T$ is the absolute temperature, $\Lambda = h/(2\pi mkT)^{1/2}$ represents the thermal wavelength with $h$ and $m$ standing for, respectively, the Planck constant and the mass of the Yukawa sphere.

To derive the excess Helmholtz energy functional due to both hard-sphere repulsion and van der Waals attraction, we incorporate the modified fundamental-measure theory (MFMT) developed by Yu and Wu[38,39] with Rosenfeld's perturbative method.[45]

$$F^{\text{ex}}[\rho(\mathbf{r})] = kT \int \Phi^{\text{hs}}[n_\alpha(\mathbf{r})]\, d\mathbf{r} + F^{\text{ex}}_{\text{att}}[\rho(\mathbf{r})] \tag{5}$$

where $\Phi^{\text{hs}}[\rho(\mathbf{r})]$ is the excess Helmholtz free-energy density due to hard-core repulsion, and $n_\alpha(\mathbf{r})$ is the weighted density defined as

$$n_\alpha(\mathbf{r}) = \int d\mathbf{r}'\rho(\mathbf{r}')w^{(\alpha)}(\mathbf{r} - \mathbf{r}') \tag{6}$$

where $\alpha = 0$, 1, 2, 3, V1, and V2. The weight functions, $w^{(\alpha)}(r)$, are given by[38,39,45,46]

$$w^{(2)}(r) = \pi\sigma^2 w^{(0)}(r) = 2\pi\sigma w^{(1)}(r) = \delta(\sigma/2 - r) \tag{7}$$

$$w^{(3)}(r) = \Theta(\sigma/2 - r) \tag{8}$$

$$\mathbf{w}^{(V2)}(\mathbf{r}) = 2\pi\sigma\mathbf{w}^{(V1)}(\mathbf{r}) = (\mathbf{r}/r)\delta(\sigma/2 - r) \tag{9}$$

where $\Theta(r)$ is the Heaviside step function, and $\delta(r)$ denotes the Dirac delta function. Integration of the two scalar functions, $w^{(2)}(r)$ and $w^{(3)}(r)$, with respect to the position gives the particle surface area and volume, respectively, and integration of the vector function $\mathbf{w}^{(V2)}(\mathbf{r})$ is related to the gradient across a sphere

in the **r** direction. In the MFMT, the Helmholtz free-energy density consists of terms dependent on scalar- and vector-weighted densities,

$$\Phi^{hs}[n_\alpha(\mathbf{r})] = \Phi^{hs(S)}[n_\alpha(\mathbf{r})] + \Phi^{hs(V)}[n_\alpha(\mathbf{r})] \quad (10)$$

where the superscripts (S) and (V) represent the contributions from scalar- and vector-weighted densities, respectively. The scalar Helmholtz energy density is given by

$$\Phi^{hs(S)}[n_\alpha(\mathbf{r})] = -n_0 \ln(1-n_3) + \frac{n_1 n_2}{1-n_3} + \frac{{n_2}^3 \ln(1-n_3)}{36\pi {n_3}^2} + \frac{{n_2}^3}{36\pi n_3 (1-n_3)^2} \quad (11)$$

and the vector part is expressed by

$$\Phi^{hs(V)}[n_\alpha(\mathbf{r})] = -\frac{\mathbf{n}_{V1}\cdot\mathbf{n}_{V2}}{1-n_3} - \frac{n_2 \mathbf{n}_{V2}\cdot\mathbf{n}_{V2} \ln(1-n_3)}{12\pi {n_3}^2} - \frac{n_2 \mathbf{n}_{V2}\cdot\mathbf{n}_{V2}}{12\pi n_3 (1-n_3)^2} \quad (12)$$

In eq 12, $\mathbf{n}_{V1}$ and $\mathbf{n}_{V2}$ are vectors, and $\mathbf{n}_{V1}\cdot\mathbf{n}_{V2}$ and $\mathbf{n}_{V2}\cdot\mathbf{n}_{V2}$ are dot products. In the limit of a homogeneous fluid, the two vector-weighted densities $\mathbf{n}_{V1}$ and $\mathbf{n}_{V2}$ vanish, and the Helmholtz free-energy density becomes identical to that derived from the Carnahan−Starling equation of state.[47] It should be pointed out that the tensor-weighted density is introduced to describe the structures of the hard sphere crystal by Tarazona.[48] However, for hard sphere fluid, our previous work[38,39] shows that the Helmholtz free-energy functional without tensor-weighted density reproduces very accurate density profiles. Therefore we also neglect the tensor-weighted density in this work.

To obtain the contribution of a long-range van der Waals interaction to the excess Helmholtz energy functional, Rosenfeld assumed that it could be perturbatively constructed around that for the bulk fluid at equilibrium. According to Rosenfeld,[45] we can make a functional Taylor expansion of the residual Helmholtz energy functional around that for a uniform fluid, i.e.,

$$F_{att}^{ex}[\rho(\mathbf{r})] = F_{att}^{ex}(\rho_b) + \int d\mathbf{r} \frac{\delta F_{att}^{ex}}{\delta\rho(\mathbf{r})}\Delta\rho(\mathbf{r}) + \frac{1}{2}\int d\mathbf{r}\, d\mathbf{r}' \frac{\delta^2 F_{att}^{ex}}{\delta\rho(\mathbf{r})\delta\rho(\mathbf{r}')}\Delta\rho(\mathbf{r})\Delta\rho(\mathbf{r}') + \cdots \quad (13)$$

where $\Delta\rho(\mathbf{r}) = \rho(\mathbf{r}) - \rho_b$ and $\rho_b$ is the bulk density. The bulk DCF due to the residual attraction are defined as

$$\Delta C_{att}^{(1)b} = -\beta \frac{\delta F_{att}^{ex}}{\delta\rho(\mathbf{r})} = -\beta\mu_{att}^{ex} \quad (14)$$

$$\Delta C_{att}^{(2)b}(|\mathbf{r}'-\mathbf{r}|) = -\beta \frac{\delta^2 F_{att}^{ex}}{\delta\rho(\mathbf{r})\delta\rho(\mathbf{r}')} \quad (15)$$

where $\beta = 1/kT$ and $\mu_{att}^{ex}$ is the dispersive part of the excess chemical potential. If we neglect all higher-order terms $\Delta C_{att}^{(n)b}$ ($n > 2$) in eq 13, $F_{att}^{ex}[\rho(\mathbf{r})]$ becomes

$$F_{att}^{ex}[\rho(\mathbf{r})] = F_{att}^{ex}(\rho_b) + \mu_{att}^{ex}\int d\mathbf{r}\Delta\rho(\mathbf{r}) - \frac{kT}{2}\int d\mathbf{r}\, d\mathbf{r}'\Delta C_{att}^{(2)b}(|\mathbf{r}'-\mathbf{r}|)\Delta\rho(\mathbf{r})\Delta\rho(\mathbf{r}') + \cdots \quad (16)$$

Equation 16 shows that the perturbative method is completely free of any weighted density and of any higher-order DCFs. Considering the system composed of particles interacting via the hard-core multi-Yukawa potential, $\Delta C_{att}^{(2)b}(|\mathbf{r}'-\mathbf{r}|)$ is given by

$$\Delta C_{att}^{(2)b}(|\mathbf{r}'-\mathbf{r}|) = C_{MY}^{(2)b}(|\mathbf{r}'-\mathbf{r}|) - C_{hs}^{(2)b}(|\mathbf{r}'-\mathbf{r}|) \quad (17)$$

where $C_{MY}^{(2)b}(|\mathbf{r}'-\mathbf{r}|)$ and $C_{hs}^{(2)b}(|\mathbf{r}'-\mathbf{r}|)$ are the bulk second-order DCFs of a hard-core multi-Yukawa fluid and a hard-sphere fluid, respectively. Their analytical expressions can be obtained by solving the Ornstein−Zernike (OZ) equation within proper approximation closures. For the hard-core multi-Yukawa fluid, the most popular approach is to calculate $\Delta C_{att}^{(2)b}(|\mathbf{r}'-\mathbf{r}|)$ from the mean spherical approximation (MSA) due to its analytical expression in reasonable accuracy. However, the parameters in the expression of $\Delta C_{att}^{(2)b}(|\mathbf{r}'-\mathbf{r}|)$ are $3M$ functions of bulk density $\rho_b$, energy parameter $\epsilon_i$, and screening parameters $\lambda_i$, and can be only obtained by solving $3M$-coupled nonlinear equations.[29] This makes the calculation complicated for the multi-Yukawa fluid. Alternatively, the analytical expression of $\Delta C_{att}^{(2)b}(|\mathbf{r}'-\mathbf{r}|)$ obtained from the first-order MSA[44] is selected in this work, i.e.,

$$\Delta C_{att}^{(2)}(r) = \begin{cases} \sum_{i=1}^{M} \beta\epsilon_i \dfrac{e^{-\lambda_i(r-\sigma)/\sigma}}{r/\sigma} & , r > \sigma \\ \sum_{i=1}^{M} Y(r,\epsilon_i,\lambda_i) & , r \le \sigma \end{cases} \quad (18)$$

where

$$Y(r,\epsilon_i,\lambda_i) = \beta\epsilon_i\left[\frac{\sigma\, e^{-\lambda_i(r-\sigma)/\sigma}}{r} - Q(\lambda_i)P(r,\lambda_i)\right] \quad (19)$$

$$Q(t) = [S(t) + 12\eta L(t)e^{-t}]^{-2} \quad (20)$$

$$S(t) = \Delta^2 t^3 + 6\eta\Delta t^2 + 18\eta^2 t - 12\eta(1+2\eta) \quad (21)$$

$$L(t) = (1+\eta/2)t + 1 + 2\eta \quad (22)$$

with $\eta = \pi\rho_b\sigma^3/6$, $\Delta = 1-\eta$, $t = \lambda_i$ and $P(r, \lambda_i)$ defined as

$$P(r,t) = S^2(t)\frac{\sigma e^{-t(r-\sigma)/\sigma}}{r} + 144\eta^2 L^2(t)\frac{\sigma e^{t(r-\sigma)/\sigma}}{r} - 12\eta^2[(1+2\eta)^2 t^4 + \Delta(1+2\eta)t^5]r^3/\sigma^3 + 12\eta[S(t)L(t)t^2 - \Delta^2(1+\eta/2)t^6]r/\sigma - 24\eta[(1+2\eta)^2 t^4 + \Delta(1+2\eta)t^5] + 24\eta S(t)L(t)\sigma/r \quad (23)$$

The equilibrium density distribution for the hard-core multi-Yukawa fluid is obtained by minimization of the grand potential functional $\Omega[\rho(\mathbf{r})]$, which yields

$$\ln\left[\frac{\rho(\mathbf{r})}{\rho_b}\right] = \beta\left[\mu_{hs}^{ex} - \int d\mathbf{r}'\sum_\alpha \frac{\partial\Phi^{hs}}{\partial n_\alpha} w^{(\alpha)}(\mathbf{r}'-\mathbf{r})\right] - \beta V^{ext}(\mathbf{r}) + \int d\mathbf{r}'\Delta C_{att}^{(2)b}(|\mathbf{r}'-\mathbf{r}|)\Delta\rho(\mathbf{r}') \quad (24)$$

where $\mu_{hs}^{ex}$ is the hard-sphere part of the chemical potential,

which can be obtained from the Carnahan−Starling equation of state[47]

$$\beta\mu_{hs}^{ex} = \frac{\eta(8 - 9\eta + 3\eta^2)}{(1-\eta)^3} \tag{25}$$

When the hard-core multi-Yukawa fluid is confined in a slit pore or around a fixed spherical particle, the density profiles vary only in the *z*-direction or *r*-direction, i.e., $\rho_i(\mathbf{r}) = \rho_i(z)$ or $\rho_i(\mathbf{r}) = \rho_i(r)$, and can be solved from eq 24 by using the Picard-type iterative method. In the calculation, the weighted densities and the integrals in eq 24 are evaluated by using the trapezoidal rule with the step size $\Delta z$ or $\Delta r = 0.005\sigma$, and the iteration repeats until the percentage change is smaller than 0.001 at all points.

## III. Monte Carlo Simulation

To test the performance of the DFT established above, the grand canonical ensemble Monte Carlo (GCMC) simulations are carried out in this work. The details of the simulations have been described elsewhere.[35] The GCMC simulations are performed with the excess chemical potential obtained from the canonical ensemble Monte Carlo (CMC) simulations by using the Widom test particle method. The simulated fluids are confined between two parallel walls with the distance of $10\sigma$. The simulation box is cubic ($10\sigma \times 10\sigma \times 10\sigma$), and the cutoff distance of the Yukawa tails is set to be $5\sigma$. The usual periodic boundary conditions and minimum imagine conventions are applied in the directions parallel to the walls. The density profiles of the hard-core two-, three-, and four-Yukawa fluids confined in the slitlike pores at different temperatures and densities are simulated in this work. In addition, the adsorption isotherms of the hard-core two-Yukawa fluid in the slitlike pores are also obtained by using the GCMC simulations.

## IV. Results and Discussions

**A. Hard-Core Multi-Yukawa Fluid in a Slitlike Pore.** We first discuss the density distributions of a hard-core multi-Yukawa fluid confined in a slitlike pore under various conditions. In this case, the external potential from the parallel walls can be expressed as

$$V^{ext}(z) = \begin{cases} W(z) + W(H-z) & \sigma/2 \le z \le H - \sigma/2 \\ \infty & \text{otherwise} \end{cases} \tag{26}$$

where

$$W(z) = -\epsilon_W \exp\{-\lambda_W(z - \sigma/2)/\sigma\} \tag{27}$$

where $\epsilon_W$ is the energy parameter of the wall, $\lambda_W$ is the screening length of Yukawa tail for the wall, *z* is the perpendicular distance from the left wall and *H* is the width of the slitlike pore. Throughout this work, the screening length for the wall is $\lambda_W = 1.8$, the width of the pore is $H = 10\sigma$, and the reduced temperature is defined as $T^* = kT/\epsilon_1$.

In Figures 1−3, the density profiles predicted from the present DFT are compared with those from the GCMC simulations carried out in this work for the two-Yukawa fluid ($\lambda_1 = 2.8647$, $\lambda_2 = 13.5485$, and $\epsilon_2/\epsilon_1 = -1.4466$) in a slitlike pore at temperature $T^* = 4.0$, 1.25, and 0.6, respectively. In this case, the two-Yukawa fluid mimics the Lennard−Jones potential, which is repulsive near the contact distance but becomes attractive at long enough distance. For each density, two wall energy parameters $\epsilon_W/kT = 0$ and 1.0 are considered. Figures 1 and 2 suggest that the higher the wall energy parameter or the bulk density is, the larger the magnitude of the density oscillation. The density profiles shift toward the wall as the density is increased, and there is a significant accumulation of spheres near the wall at high bulk density and/or large value of $\epsilon_W$. Both the present DFT and MF theories predict the density profile well except for slightly overestimating the contact density from the MF theory at $T^* = 1.25$ and $\rho_b\sigma^3 = 0.4$. It should be mentioned that the MF theory used here is implemented by using the MFMT for the hard-core repulsion.

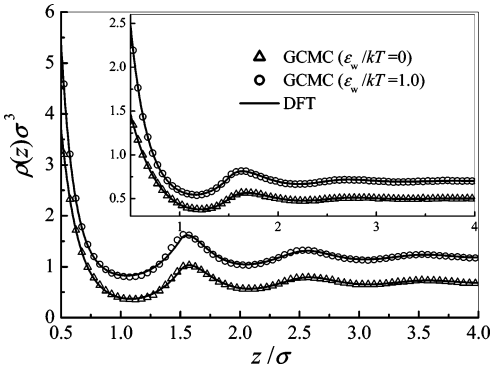


**Figure 1.** Reduced density profiles of a hard-core two-Yukawa fluid ($\lambda_1 = 2.8647$, $\lambda_2 = 13.5485$, $\epsilon_2/\epsilon_1 = -1.4466$) confined in a slitlike pore with wall energy $\epsilon_W/kT = 0$ and 1.0 at reduced temperature $T^* = 4.0$ and reduced density $\rho_b\sigma^3 = 0.5$ (inset) and 0.7. The symbols and solid curves represent the results from the GCMC simulations and the DFT, respectively. To enhance visual clarity, the density profiles for $\epsilon_W/kT = 1.0$ at $\rho_b\sigma^3 = 0.5$ (inset) and 0.7 are shifted upward by 0.2 and 0.5, respectively.

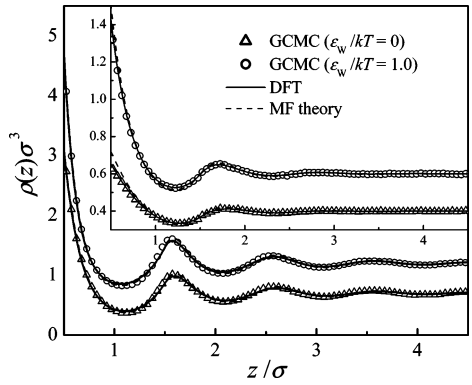


**Figure 2.** Reduced density profiles of a hard-core two-Yukawa fluid ($\lambda_1 = 2.8647$, $\lambda_2 = 13.5485$, $\epsilon_2/\epsilon_1 = -1.4466$) confined in a slitlike pore with wall energy $\epsilon_W/kT = 0$ and 1.0 at reduced temperature $T^* = 1.25$ and reduced density $\rho_b\sigma^3 = 0.4$ (inset) and 0.7. The symbols, dashed and solid curves represent the results from the GCMC simulations, MF theory and DFT, respectively. To enhance visual clarity, the density profiles for $\epsilon_W/kT = 1.0$ at $\rho_b\sigma^3 = 0.4$ (inset) and 0.7 are shifted upward by 0.2 and 0.5, respectively.

As the temperature is decreased, the density profile exhibits fewer oscillations and monotonically decreases at the approach of the nonattractive wall, as shown in Figure 3. This depletion is the result of the competition between excluded-volume and long-range attraction interaction: the former favors accumulation of spheres near the wall, while the latter holds back the spheres close to the wall. At low temperature and low density, the attractive interaction prevails and the density profile shows depletion. The comparisons of theoretical predictions with the GCMC simulation data show that the performance of the present DFT is excellent. In contrast, the MF theory overestimates the density profile in the vicinity of the wall and gives incorrect oscillatory behaviors. Figure 3 demonstrates that the MF theory

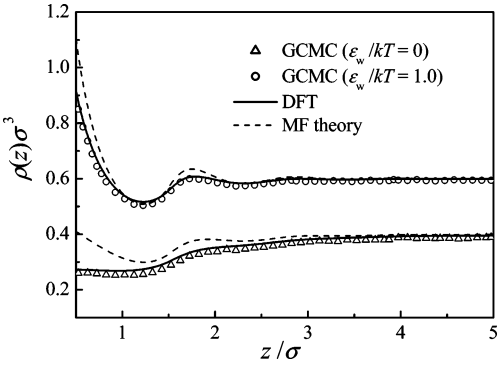


**Figure 3.** Reduced density profiles of a hard-core two-Yukawa fluid ($\lambda_1 = 2.8647$, $\lambda_2 = 13.5485$, $\epsilon_2/\epsilon_1 = -1.4466$) confined in a slitlike pore with wall energy $\epsilon_W/kT = 0$ and 1.0 at reduced temperature $T^* = 0.6$ and reduced density $\rho_b\sigma^3 = 0.4$. The symbols, dashed and solid curves represent the results from the GCMC simulations, MF theory and DFT, respectively. To enhance visual clarity, the density profile for $\epsilon_W/kT = 1.0$ is shifted upward by 0.2.

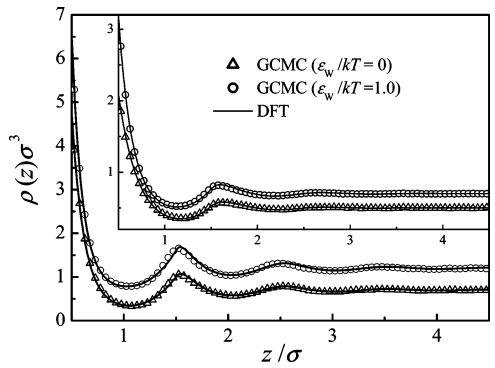


**Figure 4.** Same as in Figure 1 but $T^* = -1.25$.

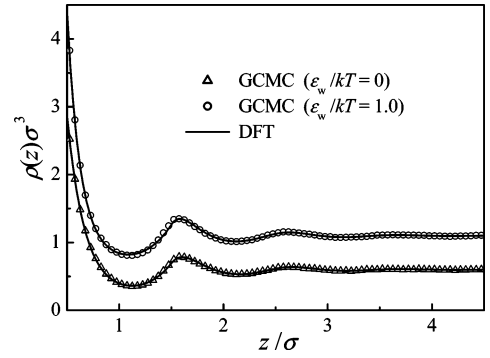


**Figure 5.** BSA density profiles of BSA−electrolyte solution confined in a slitlike pore with wall energy $\epsilon_W/kT = 0$ and 1.0 at 298.15 K, pH 4.7, and ionic strength $I = 0.1$ mol/L and reduced bulk density $\rho_b\sigma^3 = 0.6$.

is not only quantitatively unreliable but also qualitatively questionable because of its failure to describe the depletion near the wall at the low temperature. In addition, the MF theory gives too strong density oscillation for fluid with the long-range attractive force due to its neglect of the structural free-energy functional. Figure 4 presents the results of the present DFT as well as its comparisons with the GCMC simulation data under the same conditions as in Figure 1 but for $T^* = -1.25$. At this temperature, the potential is attractive at short distance but becomes repulsive at enough long distance. The density profiles are similar to those in Figure 2, but higher contact densities are observed at $T^* = -1.25$.

Figure 5 depicts the BSA density profiles of BSA−NaCl aqueous solution confined in a slitlike pore at 298.15 K, pH 4.7 and ionic strength $I = 0.1$mol/L. The interaction between

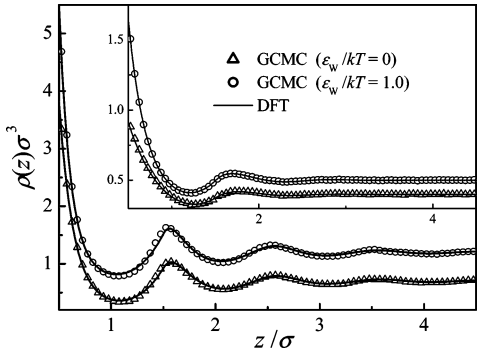


**Figure 6.** Reduced density profiles of a hard-core three-Yukawa fluid ($\lambda_1 = 1.8$, $\lambda_2 = 4.0$, $\lambda_3 = 24$; $\epsilon_2/\epsilon_1 = -1.0$; $\epsilon_3/\epsilon_1 = -1.0$) confined in a slitlike pore with wall energy $\epsilon_W/kT = 0$ and 1.0 at reduced temperature $T^* = 5.0$ and reduced density $\rho_b\sigma^3 = 0.4$ (inset) and 0.7. The symbols and solid curves represent the results from the GCMC simulations and the DFT, respectively. To enhance visual clarity, the density profiles for $\epsilon_W/kT = 1.0$ at $\rho_b\sigma^3 = 0.4$ (inset) and 0.7 are shifted upward by 0.1 and 0.5, respectively.

charged BSA surrounded by counterions includes a van der Waals attraction and the screened Coulombic repulsion, which can be expressed as two-Yukawa tails. We use $\epsilon_1/k = 91.3$ K and $\lambda_1 = 1.8$ for the van der Waals interaction and obtain the Yukawa potential parameters from the DLVO theory for the screened Coulombic repulsion, i.e.,

$$\epsilon_2 = -\frac{z_p^2 e^2}{\sigma D(1+\kappa\sigma/2)^2} \text{ and } \lambda_2 = \kappa\sigma \tag{28}$$

where $z_p$ is the charge number of BSA, $e$ is the charge of an electron, $D$ is the dielectric constant of pure water, and $\kappa$ is the Debye screening parameter, which is given by

$$\kappa^2 = \sum_i \frac{N_A c_i z_i^2 e^2}{DkT} \tag{29}$$

where $N_A$ is the Avogadro constant, $c_i$ and $z_i$ are, respectively, the molar concentration and the valence of microion $i$. Under the condition given above, the hard-core diameter and the charge number of BSA are 7.20 nm and +4.5, respectively. Then from eqs 25 and 26, we obtain $\epsilon_2/k = -141.8$ K and $\lambda_2 = 2.1132$. The density profiles of BSA in Figure 5 show some analogy to those in Figure 4, exhibiting oscillations near the wall. In both cases plotted in Figures 4 and 5, the density profiles predicted from the present DFT are in excellent agreement with those from the GCMC simulations.

In Figures 6 and 7, the density profiles from the present DFT are compared with those from the GCMC simulations for the hard-core three-Yukawa fluid with potential parameters $\lambda_1 = 1.8$, $\lambda_2 = 4.0$, $\lambda_3 = 24.0$, $\epsilon_2/\epsilon_1 = -1.0$, and $\epsilon_3/\epsilon_1 = -1.0$. In this case, there are attractive and repulsive interactions outside the hard-core, but the repulsive interactions are smaller than the attractive one. From Figures 6 and 7, we can see that the present DFT accurately reproduces the density profiles of the three-Yukawa fluid in the slitlike pore at moderate to high temperatures. When the temperature is decreased to $T^* = 0.7$ (see Figure 7), depletion is found near the nonattractive wall. Different from the case shown in Figure 3, the present DFT slightly overestimates the density at contact and the MF theory underestimates the density profiles at all positions in the pore.

Figure 8 illustrates the comparisons of the predicted density profiles with the GCMC simulation data for the four-Yukawa fluid with potential parameters $\lambda_1 = 1.8$, $\lambda_2 = 4.0$, $\lambda_3 = 8.0$,

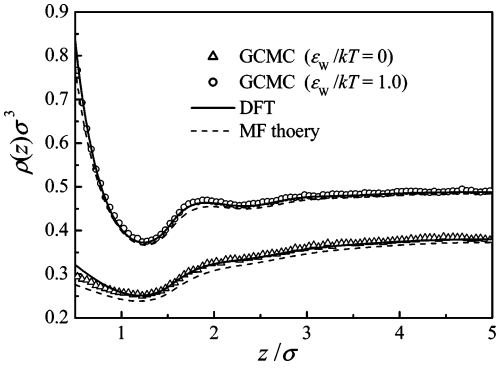


**Figure 7.** Reduced density profiles of a hard-core three-Yukawa fluid ($\lambda_1 = 1.8$, $\lambda_2 = 4.0$, $\lambda_3 = 24$; $\epsilon_2/\epsilon_1 = -1.0$; $\epsilon_3/\epsilon_1 = -1.0$) confined in a slitlike pore with wall energy $\epsilon_W/kT = 0$ and 1.0 at reduced temperature $T^* = 0.7$ and reduced density $\rho_b\sigma^3 = 0.4$. The symbols, dashed and solid curves represent the results from the GCMC simulations, MF theory and DFT, respectively. To enhance visual clarity, the density profile for $\epsilon_W/kT = 1.0$ is shifted upward by 0.1.

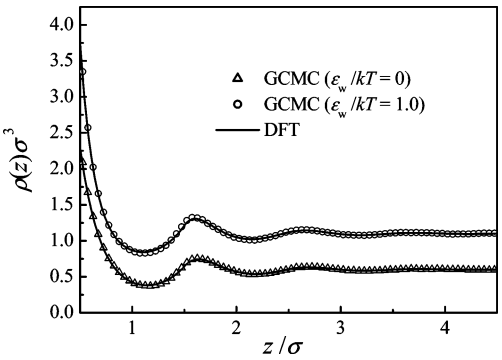


**Figure 8.** Reduced density profiles of a hard-core four-Yukawa fluid ($\lambda_1 = 1.8$, $\lambda_2 = 4.0$, $\lambda_3 = 8$, $\lambda_4 = 12$; $\epsilon_2/\epsilon_1 = -0.5$, $\epsilon_3/\epsilon_1 = -0.5$,$\epsilon_4/\epsilon_1 = -1.0$) confined in a slitlike pore with wall energy $\epsilon_W/kT = 0$ and 1.0 at reduced temperature $T^* = 3.0$ and reduced density $\rho_b\sigma^3 = 0.6$. The symbols and solid curves represent the results from the GCMC simulations and the DFT, respectively. To enhance visual clarity, the density profile for $\epsilon_W/kT = 1.0$ is shifted upward by 0.5.

$\lambda_4 = 12.0$, $\epsilon_2/\epsilon_1 = -0.5$, $\epsilon_3/\epsilon_1 = -0.5$, and $\epsilon_4/\epsilon_1 = -1.0$ at $T^* = 3.0$ and $\rho_b\sigma^3 = 0.6$. As expected, an excellent agreement between the results predicted from the present DFT and the GCMC simulation data is achieved. From all the results described above, we find that the present DFT predicts very accurate density profiles of the multi-Yukawa fluid in the slitlike pore under all the conditions considered in this work. In contrast, the MF theory may overestimate or underestimate the density profiles at low temperatures.

**B. Surface Excess.** The surface excess $\Gamma^{ex}$ is a quantity of interest in experiments. It is defined as

$$\Gamma^{ex} = \int_{\sigma/2}^{H-\sigma/2} [\rho(z) - \rho_b]\, dz \tag{30}$$

In this work, we consider the hard-core two-Yukawa fluid with potential parameters $\lambda_1 = 2.8647$, $\lambda_2 = 13.5485$, and $\epsilon_2/\epsilon_1 = -1.4466$, which is used to approximate the Lennard−Jones potential. Figure 9 depicts $\Gamma^{ex}$ as a function of bulk density at $T^* = 1.0$ for two-wall energy parameters $\epsilon_W/kT = 0$ and 1.0. For the surface without attraction, $\Gamma^{ex}$ deceases at first, and then increases rapidly as the bulk density is increased. This behavior can also be explained in terms of long-range attractive interaction and of excluded volume effects. Figure 9 shows that long-range attractive interaction is dominant at low density, and excluded volume interactions begin to play an important role at high density. As a consequence of the interplay between two

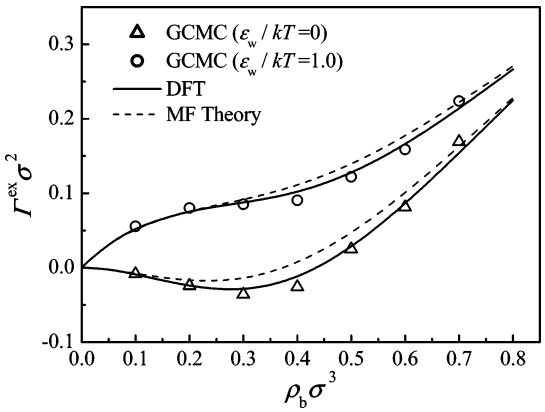


**Figure 9.** Adsorption isotherms of a hard-core two-Yukawa fluid ($\lambda_1 = 2.8647$, $\lambda_2 = 13.5485$, $\epsilon_2/\epsilon_1 = -1.4466$) confined in a slitlike pore with wall energy $\epsilon_W/kT = 0$ and 1.0 at reduced temperature $T^* = 1.0$. The symbols, dashed and solid curves represent the results from the GCMC simulation, MF theory and present DFT, respectively.

effects, $\Gamma^{ex}$ displays a nonmonotonic variation with bulk density, both in the theory and in the simulations. For attractive surfaces, the surface excess is high. The curve of $\Gamma^{ex}$ as a function of bulk density is similar to that for the surface without attraction except in the range of very low density ($\rho_b\sigma^3 < 0.1$). An interesting phenomenon is observed at very low density, i.e., $\Gamma^{ex}$ increases rapidly as the density is increased. This finding indicates that the surface attraction dominates the adsorption at very low density. The present DFT reproduces the surface excess quite well. While the trends of $\Gamma^{ex}$ predicted from the MF theory as a function of bulk density are only in qualitative agreement with the GCMC simulations, its quantitative performance remains unsatisfactory. At moderate to high densities, the MF theory predicts an adsorption excess higher than what is seen in the GCMC simulation.

**C. Radial Distribution Function.** To demonstrate the applicability of present DFT to bulk multi-Yukawa fluid, we compare the predicted radial distribution function (RDF) with the Monte Carlo simulation data for the two-Yukawa fluid with potential parameters $\lambda_1 = 1.8$, $\lambda_2 = 4.0$, and $\epsilon_2/\epsilon_1 = -3.0$. In this case, the potential is repulsive at short distances and becomes attractive at long distances. The RDF is calculated based on the idea of Percus' test-particle method. If we fix a sphere, then the external potential produced by the fixed sphere is given by

$$V^{ext}(r) = \begin{cases} \infty & r < \sigma \\ -\sum_{i=1}^{M} \dfrac{\epsilon_i \exp[-\lambda_i(r/\sigma - 1)]}{r/\sigma} & r \geq \sigma \end{cases} \tag{31}$$

If the density profile of other spheres around the fixed one is obtained from the present DFT, the RDF $g(r)$ is obtained through

$$g(r) = \rho(r)/\rho_b \tag{32}$$

Figure 10 depicts the predicted RDF for the two-Yukawa fluid at $T^* = 2.0$ and $\rho\sigma^3 = 0.8$, along with the canonical ensemble Monte Carlo (CMC) simulation data of Lin et al.[31] The agreement between the present DFT and the computer simulation is excellent, while the MF theory predicts a lower contact value and weaker oscillations when compared to the CMC simulation data. In Figure 11, we plot the contact value of RDF as a function of density at $T^* = 1.5$ and 3.0. The contact value increases monotonically with the density. The present DFT predicts a very accurate contact value of RDF, while the MF

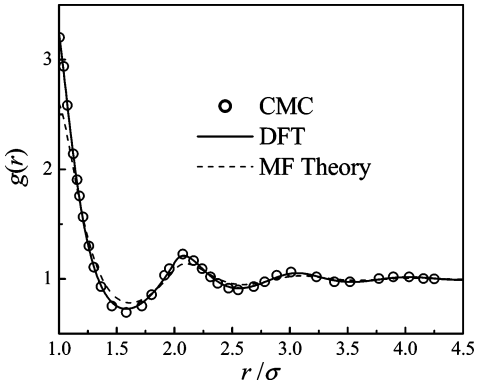


**Figure 10.** Radial distribution function of the hard-core two-Yukawa fluid ($\lambda_1 = 1.8$, $\lambda_2 = 4.0$, $\epsilon_2/\epsilon_1 = -3.0$) at reduced temperature $T^* = 2.0$ and reduced density $\rho\sigma^3 = 0.8$. The symbols, dashed and solid curves represent the results from the Monte Carlo simulation of Lin et al.,[31] MF theory and present DFT, respectively.

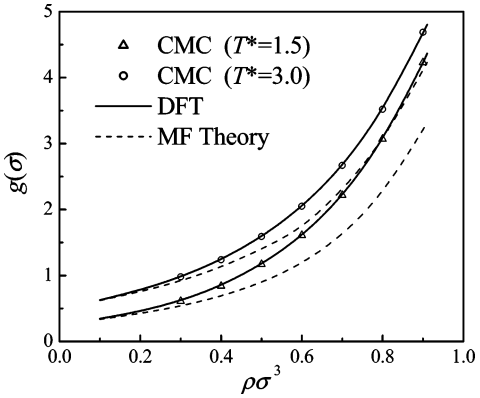


**Figure 11.** The contact value of RDF as a function of reduced bulk density for the hard-core two-Yukawa fluid ($\lambda_1 = 1.8$, $\lambda_2 = 4.0$, $\epsilon_2/\epsilon_1 = -3.0$) at reduced temperature $T^* = 1.5$ and 3.0. The symbols, dashed and solid curves represent the results from the Monte Carlo simulation of Lin et al.,[31] MF theory and present DFT, respectively.

theory substantially underestimates the contact value of RDF at both temperatures. Nevertheless, as expected, the two theories give the same limiting contact value of RDF as the density tends to zero. From Figures 10 and 11, we conclude that the present DFT is applicable to the structural and thermodynamic properties of the bulk multi-Yukawa fluid.

## V. Conclusions

Because of increasing interest in studying the phenomenon exhibited by fluid systems with a van der Waals force and a long-range repulsion, we present a density functional theory for a hard-core multi-Yukawa fluid. The excess Helmholtz free-energy functional is constructed by using the modified fundamental measure theory of Yu and Wu[38] for hard-core contribution and Rosenfeld's perturbative method for dispersion contribution. The resulting Helmholtz free-energy functional for the dispersion is a quadratic expansion with respect to the corresponding bulk fluid, in which bulk direct correlation function is the analytical solution of the Ornstein−Zernike integral equation with the first-order mean spherical approximation (FMSA) closure. The obtained theory is simple in form and easy to implement.

To validate the present DFT, grand canonical ensemble Monte Carlo (GCMC) simulations have been carried out to simulate the density profiles and surface excesses of the hard-core multi-Yukawa fluids confined in the slitlike pores. Extensive comparisons of the theoretical predictions with the GCMC simulation data show that the present DFT is quite accurate. It is capable of describing the surface depletion of multi-Yukawa fluids at low temperature. In contrast, the well-known mean-field theory overestimates or underestimates the density profiles in the vicinity of the solid surface for the multi-Yukawa fluids at low temperature and fails to account for the surface depletion in some cases.

When the present DFT is applied to the calculation of the radial distribution function for the two-Yukawa fluid, an excellent agreement between the predictions from the DFT and the simulation data is achieved. However, the MF theory substantially underestimates the radial distribution function in the vicinity of contact for the system considered in the text. It is concluded that the present DFT is comprehensively reliable and computationally efficient and can be used to predict the structural and thermodynamic properties of both inhomogeneous and homogeneous multi-Yukawa fluids. It is most promising for practical applications such as gas storage, colloidal suspensions in confining geometry, removal of various pollutants, etc.

**Acknowledgment.** The financial support of the National Natural Science Foundation of China under grant no. 20376037 and the National Basic Research Program of China under grant no. 2003CB615700 are acknowledged. F.-Q. You is thankful to Prof. J. N. Herrera for the discussion of the MSA solution for Yukawa fluid.

## References and Notes

(1) Dillon, A. C.; Jones, K. M.; Bekkedahl, T. A.; Kiang, C. H.; Bethune, D. S.; Heben, M. J. *Nature* **1997**, *386*, 377.
(2) Gast, A. P.; Russel, W. B. *Phys. Today* **1998**, *51*, 24.
(3) Frenkel, D. *Science* **2002**, *296*, 65.
(4) Henderson, D. *Fundamentals of Inhomogeneous Fluids*; Dekker: New York, 1992.
(5) Leach, A. R. *Molecular Modelling: Principles and Applications*, 1st ed.; Addison-Wesley Longman: London, 1996.
(6) Tang, Y.; Tong, Z.; Lu, B. C.-Y. *Fluid Phase Equilib.* **1997**, *134*, 21.
(7) Gonzalez-Mozuelos, P.; Alejandre, J.; Medina-Noyola, M. *J. Chem. Phys.* **1991**, *95*, 8337.
(8) Lin, Y.-Z.; Li, Y.-G.; Lu, J.-F. *J. Colloid Interface Sci.* **2001**, *239*, 58.
(9) Yu, Y.-X.; Tian, A.-W.; Gao, G.-H. *Phys. Chem. Chem. Phys.* **2005**, *7*, 2423.
(10) Liu, Y.; Chen, W.-R.; Chen, S.-H. *J. Chem. Phys.* **2005**, *122*, 044507.
(11) Wu, J.; Cao, J. *J. Phys. Chem. B* **2005**, *109*, 21342.
(12) Guerin, H. *J. Phys.: Condens. Matter* **1998**, *10*, L527.
(13) Malfois, M.; Bonnete, F.; Belloni, L.; Tardieu, A. *J. Chem. Phys.* **1996**, *105*, 3290.
(14) Waisman, E. *J. Chem. Phys.* **1973**, *59*, 495.
(15) Shukla, K. P. *J. Chem. Phys.* **2000**, *112*, 10358.
(16) van Horn, H. M. *Science* **1991**, *252*, 384.
(17) Gonzalez-Melchor, M.; Trokhymchuk, A.; Alejandre, J. *J. Chem. Phys.* **2001**, *115*, 3862.
(18) Blum, L.; Hoye, J. S. *J. Stat. Phys.* **1978**, *19*, 317.
(19) Blum, L. *J. Stat. Phys.* **1980**, *22*, 661.
(20) Duh, D.-M.; Mier-Y-Teran, L. *Mol. Phys.* **1997**, *90*, 373.
(21) Henderson, D.; Blum, L.; Nowortya, J. P. *J. Chem. Phys.* **1995**, *102*, 4973.
(22) Herrera, J. N.; Blum, L.; Garcia-LIanos, E. *J. Chem. Phys.* **1996**, *105*, 9288.
(23) Herrera, J. N.; Ruiz-Estrada, H.; Blum, L. *J. Chem. Phys.* **1996**, *104*, 6327.
(24) Vazquez, O.; Herrera, J. N.; Blum, L. *Physica* **2003**, *325*, 319.
(25) Liu, Z. P.; Li, Y.-G.; Chan, K. Y. *Ind. Eng. Chem. Res.* **2001**, *40*, 973.
(26) Tochimani, S. B.; Herrera, J. N.; Blum, L. *Physica A* **2005**, *354*, 355.
(27) Cochran, T. W.; Chiew, Y. C. *J. Chem. Phys.* **2004**, *121*, 1480.
(28) Hoye, J. S.; Stell, G.; Waisman, E. *Mol. Phys.* **1976**, *32*, 209.
(29) Hoye, J. S.; Blum, L. *J. Stat. Phys.* **1977**, *16*, 399.
(30) Lin, Y.-Z.; Li, Y.-G.; Lu, J.-F. *Mol. Phys.* **2004**, *102*, 63.
(31) Lin, Y.-Z.; Li, Y.-G.; Lu, J.-F.; Wu, W. *J. Chem. Phys.* **2002**, *117*, 10165.

(32) Sun, J. *Phys. Rev. E* **2003**, *68*, 061503.
(33) Olivares-Rivas, W.; Degreve, L.; Henderson, D.; Quintana, J. *J. Chem. Phys.* **1997**, *106*, 8160.
(34) Yi, J.-H.; Kim, S.-C. *J. Chem. Phys.* **1997**, *107*, 8147.
(35) You, F.-Q.; Yu, Y.-X.; Gao, G.-H. *J. Phys. Chem. B* **2005**, *109*, 3512.
(36) Tang, Y. *J. Chem. Phys.* **2004**, *121*, 10605.
(37) Fu, D.; Zhao, Y. *Acta Chim. Sin.* **2005**, *63*, 11.
(38) Yu, Y.-X.; Wu, J. Z. *J. Chem. Phys.* **2002**, *117*, 10156.
(39) Yu, Y.-X.; Wu, J. Z.; Xin, Y.-X.; Gao, G.-H. *J. Chem. Phys.* **2004**, *121*, 1535.
(40) Katsov, K.; Weeks, J. D. *J. Phys. Chem. B* **2001**, *105*, 6738.
(41) Katsov, K.; Weeks, J. D. *J. Phys. Chem. B* **2002**, *106*, 8429.
(42) Huang, D. M.; Chandler, D. *J. Phys. Chem. B* **2002**, *106*, 2047.
(43) Tang, Y. *J. Chem. Phys.* **2003**, *118*, 4140.
(44) Tang, Y.; Lin, Y.-Z.; Li, Y.-G. *J. Chem. Phys.* **2005**, *122*, 184505.
(45) Rosenfeld, Y. *J. Chem. Phys.* **1993**, *98*, 8126.
(46) Rosenfeld, Y. *Phys. Rev. Lett.* **1989**, *63*, 980.
(47) Carnahan, N. F.; Starling, K. E. *J. Chem. Phys.* **1969**, *51*, 635.
(48) Tarazona, P. *Phys. Rev. Lett.* **2000**, *84*, 694.